Contrail observations using NOAA-AVHRR infrared data

Hermann Mannstein and Richard Meyer
Institut für Physik der Atmosphäre
DLR Oberpfaffenhofen

Abstract

The infrared channels of the Advanced Very High Resolution Radiometer (AVHRR) onboard of the weather satellites of the NOAA series are used for the detection of contrails. A fully automated detection scheme is described which seems to identify contrails within the satellite data with a skill comparable to that of the human observers.

The algorithm is used to derive a climatology of contrail coverage for Central Europe. First results are available for the years 1995/96 and show a well marked daily and yearly cycle as well as strong regional differences of the contrail coverage. The average daytime contrail coverage of Central Europe was found to be 0.5%.

1 Introduction

High and optically thin cirrus clouds and also aged contrails may increase the net radiation at the surface. They reduce terrestrial upward radiation flux at the top of the atmosphere while albedo is only slightly enhanced. Thus an increase of high thin ice clouds may lead to warmer surface temperatures while all other cloud types lead to surface cooling [13, 2, 9].

The global mean areal coverage by contrails is not known. Bakan et al. [1] derived from visual inspection of AVHRR data a contrail coverage of the Eastern North Atlantic region and North-western Europe. They found averages around 1 % which must be related to an average coverage of natural thin cirrus clouds which reaches almost 20 % in northern midlatitudes [15].

Passive remote sensing methods can be used to recognize ice clouds, mainly by their low brightness temperatures in the thermal infrared. Ice clouds show higher transmissivity in the AVHRR-channel 4 (10.3 to 11.3 μm) than in channel 5 (11.5 to 12.5 μm). Due to smaller crystal sizes this is enhanced in young contrails [4], but in-situ measured size spectra of old widespread contrails were found to approach those of cirrus clouds [14]. Therefore contrails cannot be clearly distinguished from natural cirrus using the limited spectral information of present meteorological satellites in space without further information.

Contrails can be distinguished in satellite images by their shape: this is what enables the human eye to detect them. Natural linear features are rare.

Unfortunately the manual-interpretations are very subjective and time-consuming. They cannot be used to deliver a longtime climatology to analyze trends in contrail cloudiness nor be used over large areas. Therefore some attempts have been made to solve the problem by various image processing algorithms. Most algorithms use an idea of Lee [8] who showed that contrails appear very bright in images of brightness temperature difference (channel 4 - channel 5).

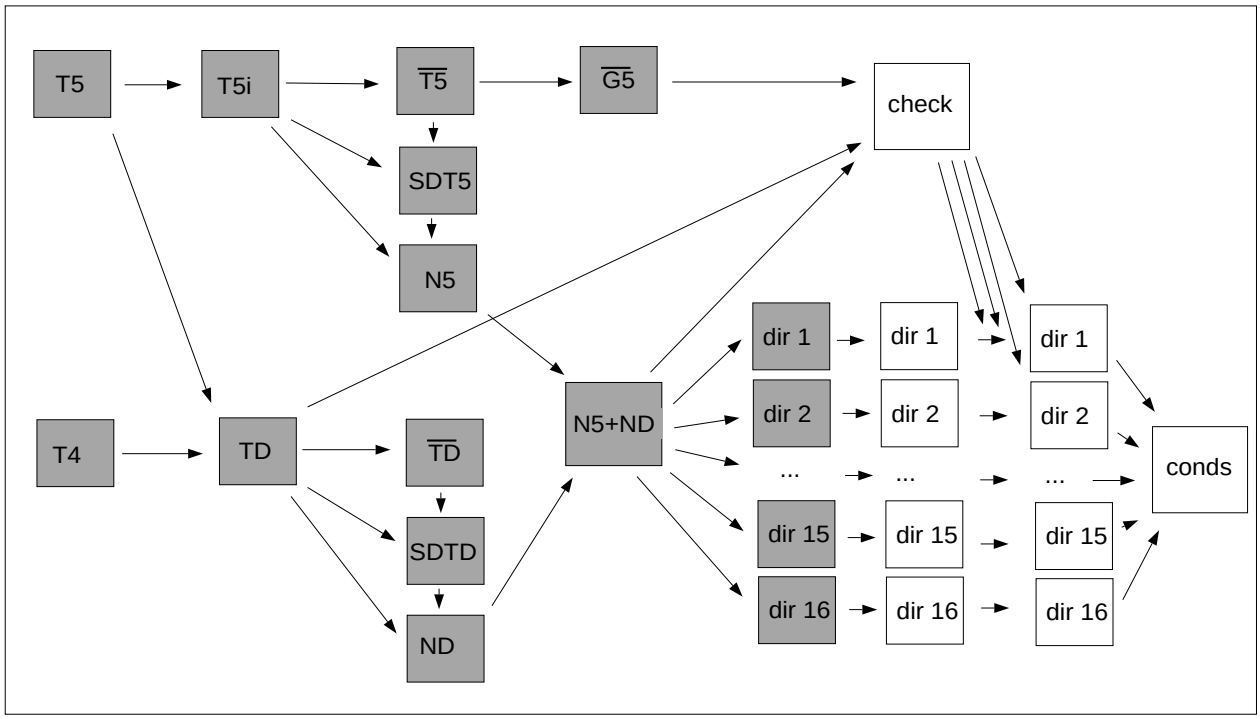

Figure 1: *Data flow for the contrail detection scheme.*

Here we describe a new algorithm that is as far as we know the first that is able to work operationally without manual interference. We present some results of the operational contrail detection. Finally, we will discuss the differences in recognizing contrails by man and machine and the limits of contrail detection efficiency.

2 Contrail Detection Algorithm

The scheme presented here is the latest stage of an algorithm development aiming to detect contrails in AVHRR data automatically. Earlier work has been described by [3] and [10]

Different tests are combined to avoid misdetections. Independence from the properties of a single scene is achieved by normalizing the data on a regional scale.

The logical structure of the data flow is drawn in figure 1. Figure 2 shows an extreme case of contrail occurence over Denmark, southern Sweden, northern Germany and the western part of Poland. This small part of an AVHRR scene is used in the following to illustrate the major steps of the contrail detection algorithm. The chosen scene contains many coastlines which make this pattern recognition task much harder than over open sea.

2.1 Description of Algorithm

Contrails mostly are best visible for human observers in a display of the temperature difference between channels 4 and 5 (TD, figure 3).. But also cloud edges and surface features appear

as bright lines. This does not happen in the temperature images (figure 2). Because of better contrasts we take the equivalent blackbody temperature derived from channel 5 ($T5$) additionally to the temperature difference (TD) as input data for the detection algorithm. To avoid interference with artifacts produced by remapping we use the data in the original satellite projection.

To be able to use constant thresholds for all data, a local standard deviation defined over a rotational symmetric gauss filtered region given by: $SDT5 = \sqrt{\overline{(T5i - \overline{T5})^2}}$ (figure 4) and $SDTD = \sqrt{\overline{(TD - \overline{TD})^2}}$

is used to normalize the data:

$$N5 = \frac{(T5i - \overline{T5})}{(SDT5 + 0.1\mathrm{K})}, \quad (1)$$

$$ND = \frac{(TD - \overline{TD})}{(SDTD + 0.1\mathrm{K})}. \quad (2)$$

Furtheron, we use the sum of the normalized images $N = N5 + ND$ to avoid the interpretation of boundary layer cloud streets as contrails. These opaque clouds are usually colder then the surrounding, while the interstitial often semi-transparent regions then show high values of TD. Adding the normalized images cancels these effects.

N is then convolved with a line filter of 19 x 19 pixels in 16 different directions (similar to [6]). Some filter-kernels are displayed in figure 11. The result of the line filtering for an angle of 45°is shown in figure 8.

Because of the normalization of the input data, a single threshold is sufficient to isolate connected regions. These are now treated as separate objects which might be contrails. Each of these objects is now checked against the mask derived as follows:

In a 15 x 15 pixel vicinity we calculate the large scale maximum gradient for $T5$ ($\overline{G5}$, figure 6). From $\overline{G5}$, $N5$, ND and TD we derive a mask (*check*) shown in figure 7 which marks all pixels fulfilling each of the following requirements:

$$N > 1.5, \quad (3)$$

$$\overline{G5} < 2 \cdot SDT5 + 1\mathrm{K}, \quad (4)$$

$$TD > 0.2\mathrm{K}. \quad (5)$$

The threshold of 1.5 in condition (3) depends on the type of normalization. It selects pixels which are brighter then the surrounding. Cloud edges and sometimes also shorelines show a high TD signal. Condition (4) applies an upper limit to the large scale gradient of the temperature image depending on the regional standard deviation to eliminate such lines before further processing.

To be regarded as a contrail, the objects have to fulfill the following criteria:

$$\text{number of pixels} > 10, \quad (6)$$

$$\text{length} > 15 \text{ pixels}, \quad (7)$$

$$\text{correlation of the pixel coordinates to a straight line} > 0.975. \quad (8)$$

Figure 7 displays the mask after applying conditions (6), (7) and (8) to the 45°filter direction.

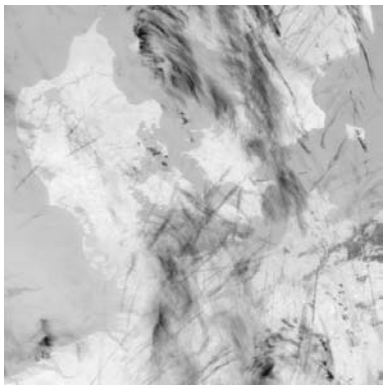

Figure 2: *NOAA-12, Temperature Channel 5 ($T5$), May 4th, 1995, 07:43 UT.*

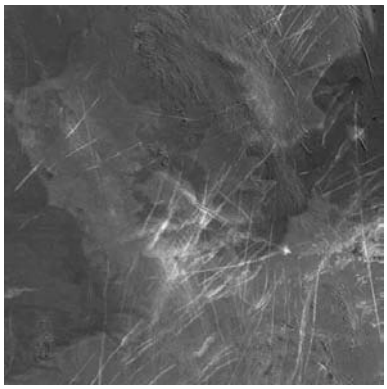

Figure 3: *NOAA-12, Temperature difference (TD), May 4th, 1995, 07:43 UT.*

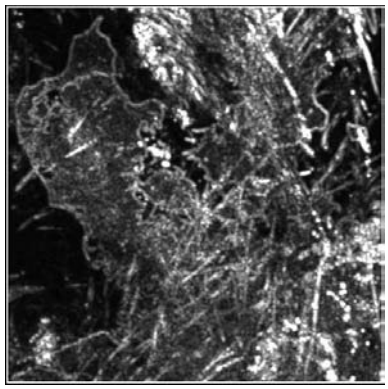

Figure 4: *Regional standard deviation ($SDT5$) of $T5$.*

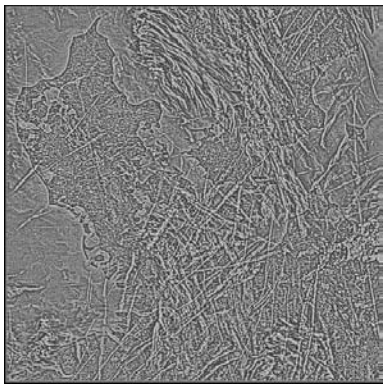

Figure 5: *Normalized temperature $N5$ (channel 5).*

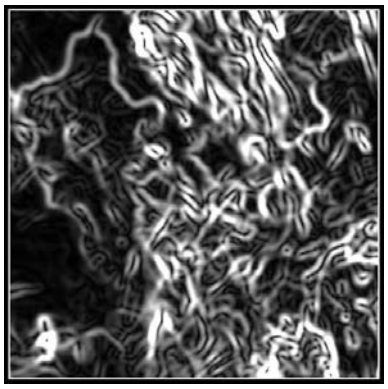

Figure 6: *Large scale maximum gradient of $T5$ ($\overline{G5}$).*

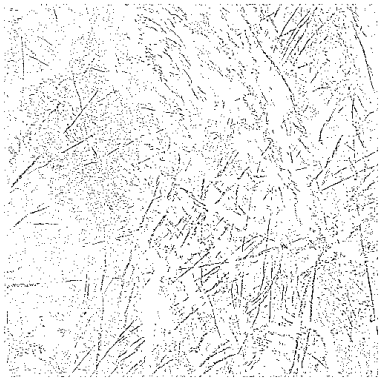

Figure 7: *First guess mask for detection of contrails at full resolution (no wide objects).*

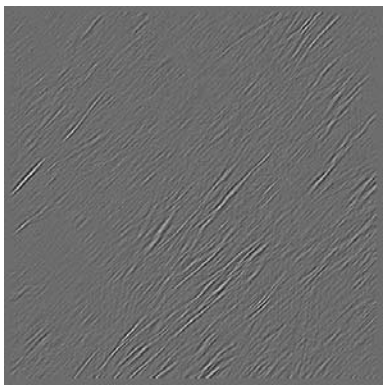

Figure 8: *Sum of normalized images N convolved with line detection kernel for 45°.*

Figure 9: *Contrails derived from direction 45° at full resolution.*

Figure 10: *Result of the contrail detection scheme (contrail clusters grey).*

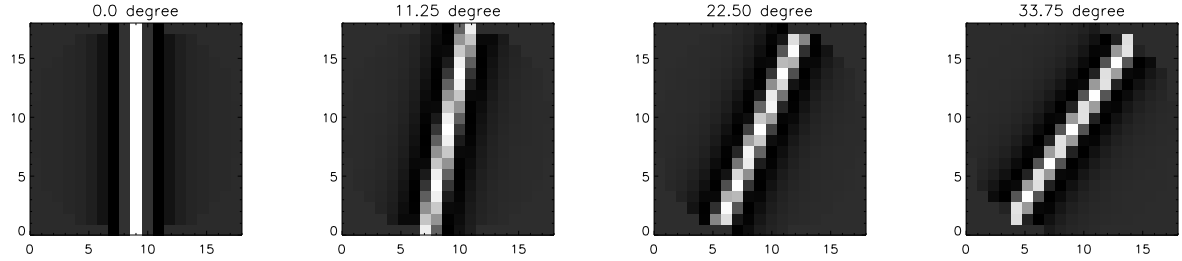

Figure 11: *Example of the first four kernels for line filtering.*

This filtering and testing procedures are repeated for all 16 directions. The results for each direction (e.g. figure 9) are added to the binary contrail array.

This scheme mainly marks contrails of a width of 1 or 2 pixels. To detect wider contrails the whole algorithm is then applied to an image reduced by factor 2 using neighborhood averaging. The results of this step are again added to the final binary contrail mask (figure 10).

The parameters in the requirements above were fixed by an evolutionary algorithm which maximized the correlation of the resulting mask with the visual analysis of some test cases.

3 Results

3.1 Actual AVHRR-detected Contrail Coverage

The contrail detection algorithm is applied to AVHRR-data preprocessed by the APOLLO scheme [5, 7] for a 1440 x 2048 pixel area covering Central Europe (figure 12). The processing time for such a scene is less than 30 min on an Ultra Sparc 2 machine.

In figure 12 all derived noon (12:30 UT $\pm$ 70 min) contrail masks for 1996 are superimposed. It can be seen that the observed contrails accumulate mainly close to and in direction of the major flight routes.

Figure 12 indicates that the algorithm is robust to misdetections. Counts of more than 10 we get for only 25 pixels in the whole image. To derive the regional AVHRR-derived contrail coverage *cc* we take into account the local contrail coverages in a 100 x 100 pixel surrounding. We calculate *cc* by filtering with a circular gauss-kernel of 50 pixels FWHM (full width half mean). This should represent the average proportion of the sky where contrails can be seen from a ground-based observer and weight it in a simple way according to their potential influence on net radiation.

Comparing the frequency of AVHRR-derived contrail coverage *cc* to the pattern of the standard deviation of temperatures in channel 5 for a 5 x 5 pixel kernel 14 we recognize a strong relationship. Above sea we mostly detect higher contrail coverages than above land. A correlation coefficient of -0.55 for both images shows that thermal heterogeneity caused by ground features and lower clouds influences contrail detection rate as expected from the normalization within the algorithm.

Viewing contrail coverages *cc* above the Alps we recognize that obviously above a certain value of

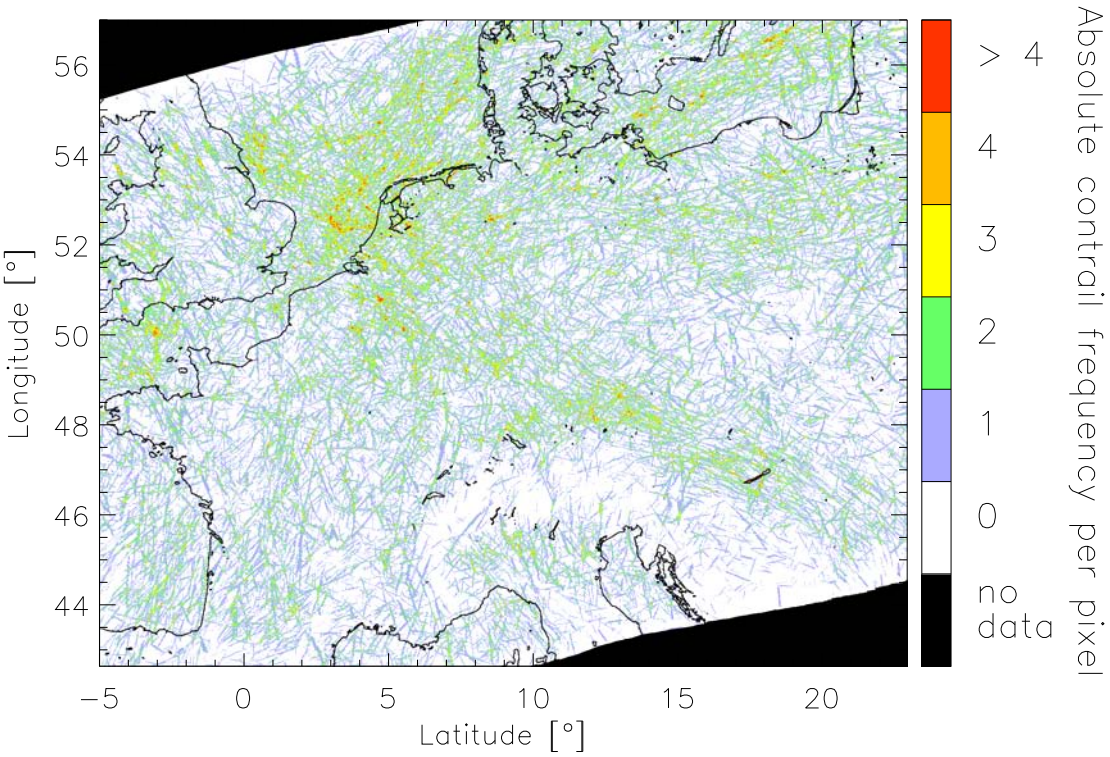

Figure 12: *Stacked contrail masks of 1996 indicate frequency and predominant bearing of air-traffic (derived from 357 AVHRR noon-passages).*

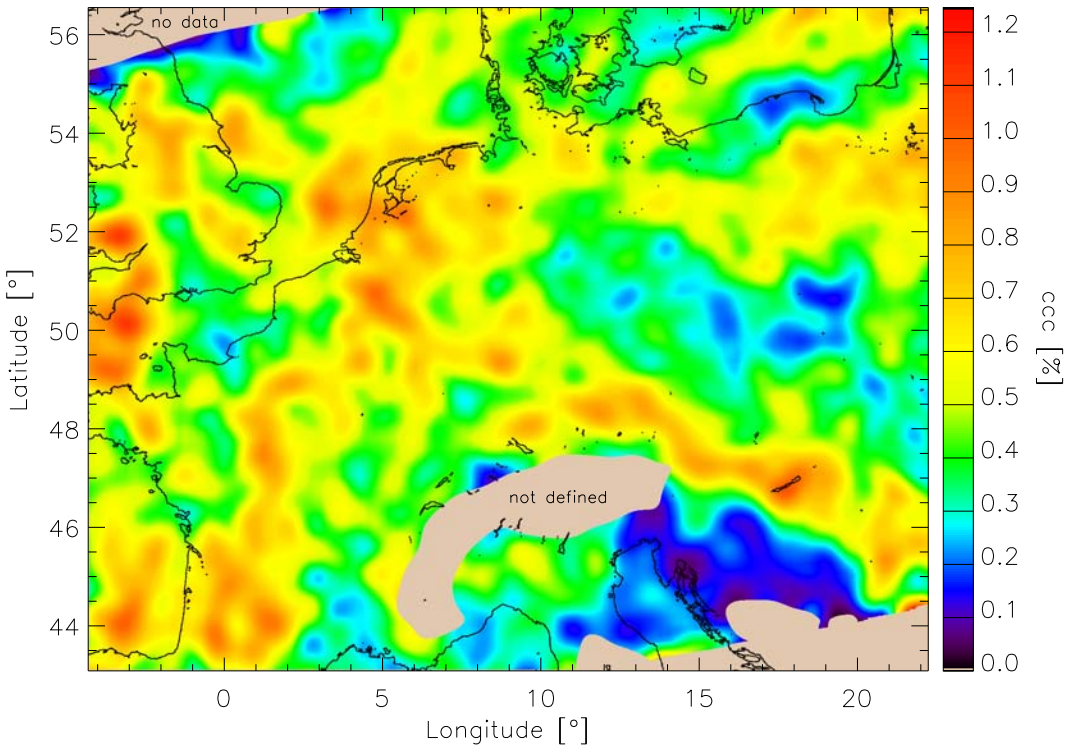

Figure 13: *Annual AVHRR-derived heterogeneity-corrected contrail coverage ccc at noon for 1996.*

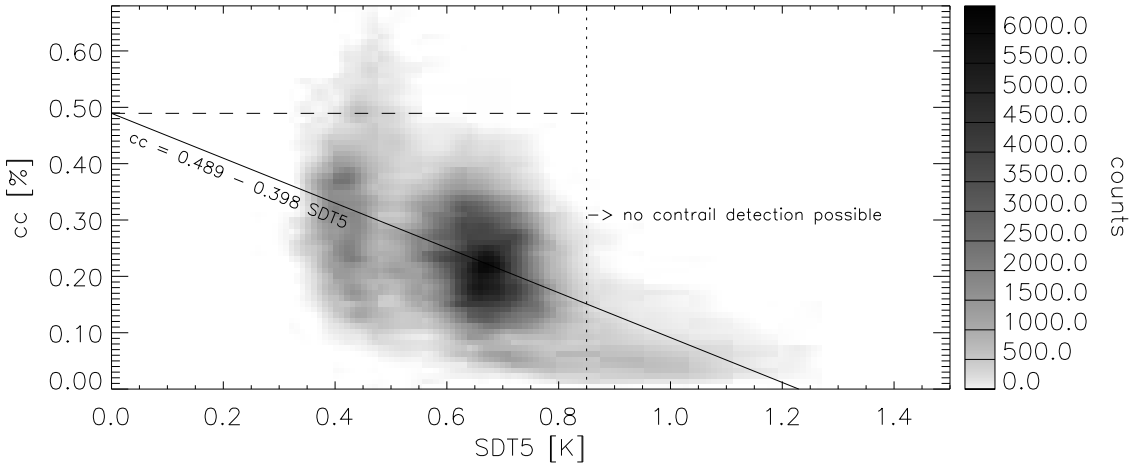

Figure 14: *2D-histogram of the standard deviation of temperatures in channel 5 for a 5 x 5 surrounding against AVHRR-derived uncorrected regional contrail coverage cc.*

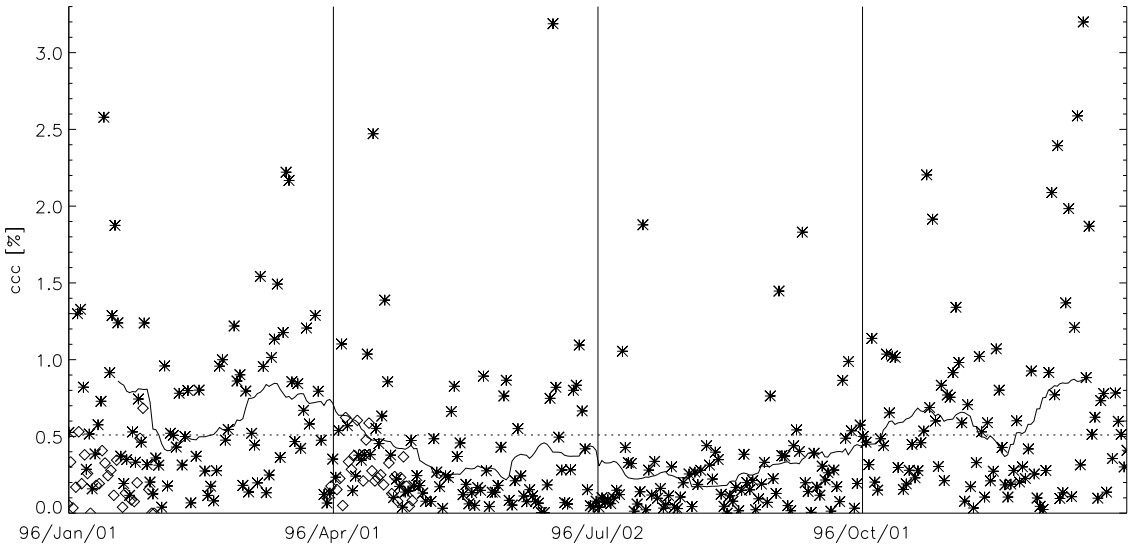

Figure 15: *Average AVHRR-derived corrected contrail coverage for the box 0°E to 20°E, 48°N to 55°N. Asterisks are noon passages, diamonds nighttime passages. The solid line shows the 30d-floating average, the dotted line marks the annual average for daytime. (Plotted are all values where data coverage was higher than 70 %. The absolute maximum of 5.6 % at January 14th is not shown.)*

$SDT5$ we hardly can detect any contrails. To avoid this effect we cut off all pixels where $SDT5$ exceeds 0.85 K (figure 14). Because we can assume that airtraffic and atmospheric conditions which allow formation of persistent contrails are not correlated to $SDT5$, we may correct cc by $SDT5$. Applying a linear regression we raise all values of regional contrail coverage according to

$$ccc = \frac{1}{1-0.397/0.489 \cdot \overline{SDT5}} \cdot cc(\overline{SDT5} < 0.85K) \tag{9}$$

to the heterogeneity-corrected AVHRR-derived regional contrail coverage *ccc* where $\overline{SDT5}$ is Gauss-filtered like *cc*. This widely removes influence of $SDT5$ ($\overline{SDT5}$ to *ccc* correlation coefficient: -0.01) as can be seen in figure 13 but strongly enhances average contrail cloudiness by extrapolation to a fictitious value of $SDT5 = 0$ K where the algorithm would work best. This correction results in an average *ccc* of 0.5 % for the observed area which approximately doubles *cc* in average.

The average for the corrected daytime contrail coverage *ccc* in the whole image (figure 13) amounts to 0.5 % $\pm$ 0.25 % in the year 1996. The spatial pattern of the algorithm-derived contrail coverage agrees with the contrail observations by Bakan et al. [1]. They also obtained the maxima in the North-Atlantic flight corridor with declining contrail cloudiness to the Eastern and Southern parts of Europe.

Some heavily flown routes can still be recognized in figure 13. Maxima of contrail coverage of 1.0 % and higher are found over Wales, The Channel and in the Balaton region.

Figure 15 shows the daily variation of the average contrail coverage in the box 0°E to 20°E, 48°N to 55°N. To derive values comparable to figure 13 we applied the heterogeneity-correction by the annual average of $\overline{SDT5}$ in this box. Thereafter the daily contrail coverage *ccc* varied from 0.0 % up to 5.7 % at a standard deviation of 0.6 %.

For the absolute values of daily contrail coverage *ccc* we estimate an error in the order of a factor 2. As the 30d-floating average in figure 15 suggests, there are noticeable annual variations with a *ccc*-minimum below 0.2 % during summer and a *ccc*-maximum close to 0.9 % during winter and spring. But temporal varying detection efficiency might have influenced this results. E.g. higher surface temperature contrasts in summer may have led to reduced *ccc*. In winter a higher fog-frequency leading to a more homogeneous background may increase the number of AVHRR-detected contrails in certain regions.

For January and April 1996 we additionally processed night-passes of NOAA 14 (01:45 UTC *pm* 50 min). To regard higher detection efficiency during night we used the corresponding $\overline{SDT5}$-images for the heterogeneity correction. We found a mean nighttime contrail coverage *ccc* of 0.24 % , while *ccc* for the same period on daytime was 0.70 % (figure 15) Thus contrail coverage at night is about one third of the daytime noon coverage. Bakan et al. [1] reported halving of contrail cloudiness during night, which seems reasonable when not regarding different detection efficiency.

3.2 Limitations of the Scheme

If air-traffic is intensive in an area and at an altitude which is suitable for the formation of persistent contrails, many contrails appear which spread and merge. This rare but relevant situation where a considerable proportion of the sky is completely covered by contrails cannot be recognized by our pattern recognition scheme that is adapted to elongated structures. Therefore in regions with very dense traffic the contrail coverage might be underestimated.

We also do not recognize widespread fuzzy patches of old contrails which no longer show their typical shape. Minnis and Young [11] observed artificial cirrus clouds developing out of contrails, which lasted for 5 to 19 hours. The observations indicate that in some critical situations air-traffic triggers cirrus formation by adding condensation nuclei. More generally the regular addition of condensation nuclei by aircraft emissions favors cirrus formation and persistence [12]. Wang et al. [15] show that the occurance of high sub-visible clouds in northern midlatitudes is almost a factor of 2 higher than that in southern midlatitudes. The tendency for an increase in cirrus coverage will

require analysis using a cirrus cloud climatology.

Also, single contrails smaller than half a pixel in width are very unlikely to be recognized especially if they are also optically thin. On the other hand such contrails will have a low impact on the net radiation and are also usually short lived.

As noted in section 3.1, misdetection of other linear structures does not seem to be a problem, but decreased detection sensitivity over extremely heterogeneous surfaces like the Alps are significant. Knowledge about actual aircraft movements and atmospheric conditions will help to interpret these situations.

The detection efficiency of contrails over mid and highlevel clouds may also be less than over warmer low clouds due to a lower temperature contrast with the background. However the higher these natural clouds are, and the less the temperature contrast, the less effect the presence of contrails has on radiation budget and the climate. Therefore the bias in the results from this limitation in the contrail detection scheme will not be as significant as an underestimate of occurance over uncovered land or sea.

4 Conclusions

The algorithm presented here is capable of the fast operational detection of persistent and roughly linearly-shaped contrails from the AVHRR-channels 4 and 5. The pattern recognition approach makes it easy to be adapted to other sensor types and to compare results. The scheme is relatively robust to misdetections of other linear structures in thermal images such as coastlines, mountain ridges and valleys or sensor line failures. The parameter settings derived are a conservative adjustment resulting in a low false alarm rate but also a low detection efficiency.

Sensitivity of the algorithm depends on the thermal homogeneity of the background. Intense temperature contrasts as can be found in high mountains strongly affect detection efficiency. When deriving the climatological parameter regional contrail coverage, it is advisable to omit those regions. To level differences in detection efficiency we adapt the derived contrail coverage by the annual average of the temperature deviation in channel 5.

The annual mean of the heterogeneity-corrected AVHRR-derived contrail coverage reached 0.5 % $\pm$ 0.25 % in 1996. We recognize strong temporal and spatial variations in contrail coverage which match those derived by Bakan et al. [1].

The scheme is not able to detect atypical contrails such as very wide spread and fuzzy ones, which are hard to distinguish from natural cirrus. The approach used also cannot recognize cases where contrails cover a large proportion of the sky destroying their individual line pattern.

The temporal variability of contrail cloudiness is known to be strong. We have presented here the results of analysis of one year's data. Work is going on to analyze a longer time-series for more robust statements on seasonal averages and trends.

Acknowledgments: This work was supported by the BMBF (German Federal Ministry for Education, Science, Research and Technology) within the DLR-BMBF project "Schadstoffe in der Luftfahrt".

References

[1] S. Bakan, M. Betancor, V. Gayler, and H. Grassl. Contrail frequency over Europe from NOAA-satellite images. *Ann. Geophys.*, 12:962–968, 1994.

[2] A. Detwiler and R. Pratt. Clear-air seeding: opportunities and strategies. *J. Wea. Mod.*, 16:46–60, 1984.

[3] T. Forkert, B. Strauss, and P. Wendling. A new algorithm for the automated detection of jet contrails from NOAA AVHRR satellite images. In *Proceedings of the 6th AVHRR Data User's Meeting, Belgirate, Italy,June 29 - July 2*, pages 513 – 519. EUMETSAT, 1993.

[4] J.-F. Gayet, G. Febvre, G. Brogniez, H. Chepfer, W. Renger, and P. Wendling. Microphysical and optical properties of cirrus and contrails: cloud field study on 13 october 1989. *J. Atmos. Sci.*, 53:126–138, 1996.

[5] G. Gesell, T. König, H. Mannstein, and K. K. T. SHARK-APOLLO quantitative satellite data analysis based on ESRIN/SHARP and DLR/APOLLO. In *Proceedings of the 6th AVHRR Data User's Meeting, Belgirate, Italy,June 29 - July 2*, pages 583 – 587. EUMETSAT, 1993.

[6] J. Hou and R. H. Bamberger. Orientation selective operators for ridge, valley and line detection in imagerey. In *ICASSP*. IEEE, 1994.

[7] K. T. Kriebel, R. W. Saunders, and G. Gesell. Optical properties of clouds derived from fully cloudy pixels. *Beitr. Phys. Atmos.*, 62:165–171, 1989.

[8] T. F. Lee. Jet contrail identification using the AVHRR infrared split window. *J. Appl. Meteor.*, 28:993–995, 1989.

[9] K. N. Liou. Influence of cirrus clouds on weather and climate processes: a global perspective. *Mon. Wea. Rev.*, 114:1167–1198, 1986.

[10] H. Mannstein. Contrail observations from space using NOAA-AVHRR data. In *"Comit'e Avion Ozone", Impact of aircraft emissions upon the atmosphere, International Colloquium Paris, 15 - 18 October*, volume II, pages 427–431, 1996.

[11] P. Minnis and D. F. Young. Transformation of contrails into cirrus during SUCCESS. *Geophys. Res. Lett.*, June 1997. submitted.

[12] U. Schumann. On the effect of emissions from aircraft engines on the state of the atmosphere. *Ann. Geophys.*, 12:365–384, 1994.

[13] G. L. Stephens and P. Webster. Clouds and climate: Sensitivity of simple systems. *J. Atmos. Sci.*, 38:235–247, 1981.

[14] B. Strauss and P. Wendling. Microphysical properties of contrails and natural cirrus clouds. In *"Comit'e Avion Ozone", Impact of aircraft emissions upon the atmosphere, International Colloquium Paris, 15 - 18 October*, volume I, pages 155–158, 1996.

[15] P.-H. Wang, P. Minnis, M. P. McCormick, S. K. Geoffrey, and K. M. Skeens. A 6-year climatology of cloud occurance frequency from Stratospheric Aerosol and Gas Experiment II observations (1985-1990). *J. Geophys. Res.*, 101(D23):29407–29429, 1996.